Pyruvate Protects against Cellular Senescence through the Control of Mitochondrial and Lysosomal Function in Dermal Fibroblasts

Jeong Yeon Kim[1,2], Sung Hoon Lee[3], Il-Hong Bae[3], Dong Wook Shin[3], Daejin Min[3], Mira Ham[3], Kyu-Han Kim[3], Tae Ryong Lee[3], Hyoung-June Kim[3], Eui Dong Son[3], Ai-Yong Lee[4], Yeong Wook Song[1,2] and In Sup Kil[3]

Mitochondrial dysfunction can drive cellular senescence, which is accompanied by changes in metabolism and increases in senescence-associated secretory phenotypes. Although pyruvate, a key metabolite for numerous aspects of metabolism, has been used as general supplement in synthetic media, the physiological function of pyruvate underlying its protective role against cellular senescence under normal conditions has remained unknown. Here, we show that extracellular pyruvate prevents senescence in normal human dermal fibroblasts through increasing the generation of oxidized nicotinamide adenine dinucleotide (NAD^+) during the conversion to lactate. Acetylated peroxisome proliferator-activated receptor gamma coactivator 1α (PGC-1α), vacuolar-type H^+-ATPaseV0A1 (v-ATPaseV0A1), NF-κB p65 subunit (RelA), and histone H3 accumulate under pyruvate deprivation conditions, resulting in the onset of senescence in normal human dermal fibroblasts through the accumulation of abnormal mitochondria generated by lysosomal inactivation-induced mitophagy defects, and through an increase in senescence-associated secretory phenotypes. Furthermore, pyruvate showed a protective effect against aging phenotypes in skin equivalents, which consist of a dermis and epidermis that act similarly to in vivo skin tissues. Our findings reveal a connection between pyruvate and mitochondrial dysfunction in the progression of senescence that is, to our knowledge, previously unreported. These results suggest that the pyruvate deprivation-induced senescence model can be used to study the connection between metabolism and senescence under normal conditions.

Journal of Investigative Dermatology (2018) ■, ■–■; doi:10.1016/j.jid.2018.05.033

INTRODUCTION

Mitochondria are multifunctional organelles that maintain cellular energy and metabolic homeostasis through the bioenergetic function of ATP production as well as the biosynthesis of various metabolites required for lipid, amino acid, and nucleotide metabolism (Martinez-Reyes et al., 2016; Yun and Finkel, 2014). Because the crosstalk between mitochondria and other organelles such as lysosome, endoplasmic reticulum, and nucleus regulates cellular homeostasis and determines cell fate for processes such as cell death, senescence, cell-cycle arrest, differentiation, or proliferation, mitochondrial dysfunction can trigger aging and age-related diseases such as metabolic diseases, neurodegenerative diseases, and cancer (Yun and Finkel, 2014). Mitochondrial quality control is thus essential for protecting cells from aging and age-related diseases, and is mainly regulated by mitophagy, a selective type of autophagy that removes abnormal mitochondria (Horan et al., 2012).

Cellular senescence, a complex biological process that causes cells to limit their rates of proliferation, is accelerated by various factors including epigenetic disorders, excessive reactive oxygen species (ROS) production, autophagic defects, and mitochondrial and lysosomal dysfunction (Kuilman et al., 2010; Lopez-Otin et al., 2013). During the aging process, decreases in NAD^+ levels through the elevation of NAD^+ consumption trigger mitochondrial dysfunction; this process can be reversed by increasing intracellular NAD^+ levels through repletion with precursors such as nicotinamide riboside or nicotinamide mononucleotide (Camacho-Pereira et al., 2016; Mills et al., 2016).

[1]*Department of Molecular Medicine and Biopharmaceutical Sciences, Graduate School of Convergence Science and Technology, Seoul National University, Seoul, Republic of Korea;* [2]*Division of Rheumatology, Department of Internal Medicine, Seoul National University Hospital, Seoul, Republic of Korea;* [3]*Basic Research & Innovation Division, Amorepacific Corporation R&D Center, Yongin-si, Gyeonggi-do, Republic of Korea; and* [4]*Department of Dermatology, Dongguk University Ilsan Hospital, Goyang-si, Gyeonggi-do, Republic of Korea*

Correspondence: Yeong Wook Song, Division of Rheumatology, Department of Internal Medicine, Seoul National University, Seoul 03080, Republic of Korea. E-mail: ysong@snu.ac.kr or In Sup Kil, Basic Research & Innovation Division, Amorepacific Corporation R&D Center, Yongin-si, Gyeonggi-do 17074, Republic of Korea. E-mail: iskil@amorepacific.com

Abbreviations: H3K9, histone H3 lysine 9; LAMP1, lysosomal-associated membrane protein 1; LDH, lactate dehydrogenase; MMP, mitochondrial membrane potential; NAD, nicotinamide adenine dinucleotide; NHDF, normal human dermal fibroblast; OCR, oxygen consumption rate; OXPHOS, oxidative phosphorylation; ROS, reactive oxygen species; SASP, senescence-associated secretory phenotype; SE, skin equivalent; siRNA, small-interfering RNA; TFEB, transcription factor EB; UCP2, uncoupling protein 2; v-ATPaseV0A1, vacuolar-type H^+-ATPaseV0A1

Received 6 November 2017; revised 17 May 2018; accepted 30 May 2018; accepted manuscript published online 28 June 2018; corrected proof published online XXX XXXX

In glucose metabolism, pyruvate is a key intermediate produced by glycolysis and can be converted to oxaloacetate via pyruvate carboxylase, to malate via malic enzyme, to acetyl-CoA via the pyruvate dehydrogenase complex, or to lactate via lactate dehydrogenase (LDH). Although pyruvate was originally thought to be an additional energy source, or required for the generation of NAD^+ using its reduced form, NADH, to maintain redox balance (Harris, 1980; King and Attardi, 1989), it was recently revealed that pyruvate supplementation induces cell proliferation through NAD^+-dependent aspartate synthesis in mitochondrial dysfunction-induced cell-cycle arrest models and protects lung fibroblasts from senescence induced by mitochondrial dysfunction by increasing the NAD^+/NADH ratio (Birsoy et al., 2015; Sullivan et al., 2015; Wiley et al., 2016). The physiological function of pyruvate underlying its protective role against cellular senescence under normal conditions has, however, remained unknown. In this study, we determined the role pyruvate plays in protecting against cellular senescence by suppressing the vicious cycle of mitochondrial-lysosomal inactivation by increasing NAD^+ generation.

RESULTS

Pyruvate prevents cellular senescence in normal human dermal fibroblasts by increasing NAD^+ generation

To gain insight into the role of pyruvate in normal human dermal fibroblasts (NHDFs) under normal conditions, we cultured NHDFs in the presence (Pyr+) or absence (Pyr−) of 1 mM pyruvate for 12 days. A functional consequence of pyruvate deprivation in the culture media was a significant decrease in the proliferation of NHDFs from day 4, and in the doubling rate at day 12 without a change of viability (Figure 1a–c). In addition, Pyr− cells showed an accumulation of cells at the G2/M phase (Figure 1d) and upregulation of $p21^{CIP1}$, a transcriptional target of p53 (Supplementary Figure S1a–c online). These data indicate that cell-cycle arrest by pyruvate deprivation is associated with p53 activation. Given that cell-cycle arrest is associated with quiescence or senescence, we analyzed the senescence markers in Pyr− cells. Pyruvate deprivation-induced senescence of NHDFs was determined based on the increase in senescence-associated β-galactosidase activity (Figure 1e), the upregulation of senescence-associated secretory phenotype (SASP) genes (Figure 1f), and a decrease in intracellular high mobility group protein B1 levels (Figure 1g). These data suggest that treatment with exogenous pyruvate prevents cellular senescence in NHDFs under extrinsic stress-free conditions.

Because the inhibition of pyruvate uptake into the mitochondria did not induce cellular senescence (Supplementary Figure 2a and b online), we focused on other functions of pyruvate such as NAD^+ generation and ROS elimination by direct scavenging. The NAD^+ precursor, nicotinamide mononucleotide, as well as α-ketobutyrate, which can also generate NAD^+ from the conversion to α-hydroxybutyrate by LDH through a mechanism similar to that of pyruvate, attenuated the decrease in cell proliferation rate and the increase in senescence-associated β-galactosidase activity due to pyruvate deprivation by increasing the NAD^+/NADH ratio, but not aspartate or antioxidant, N-acetyl cysteine (Supplementary Figure S3a–c online). These data suggest that pyruvate prevents cellular senescence in NHDFs in a manner dependent on NAD^+ generation, but not on aspartate synthesis or ROS elimination.

Pyruvate deprivation induces the accumulation of abnormal mitochondria

Next, we investigated how pyruvate deprivation induces senescence in NHDFs under normal conditions. It is well established that pyruvate prevents cell-cycle arrest or senescence under conditions of mitochondrial dysfunction (Birsoy et al., 2015; Cardaci et al., 2015; Sullivan et al., 2015; Wiley et al., 2016) and that the reduction of NAD^+ as a result of aging triggers mitochondrial dysfunction in adult muscle stem cells (Zhang et al., 2016). Therefore, we speculated that mitochondrial activity may be decreased in Pyr− cells. Interestingly, in Pyr− cells, pyruvate deprivation resulted in an approximately twofold increase in basal oxygen consumption rate (OCR) and an approximately threefold increase in maximum OCR (Figure 2a and Supplementary Figure S4a online), whereas the extracellular acidification rate was increased only slightly (Supplementary Figure S4b and c). Although the OCR in Pyr− cells was higher than that in Pyr+ cells, an increase in the ADP/ATP ratio and p-AMPK was more pronounced in the Pyr− cells than in the Pyr+ cells (Supplementary Figure S4d and e). Moreover, the mitochondrial morphology of the Pyr− cells was changed from a linear to a circular shape (Supplementary Figure S4f). These data suggest that an increase in OCR in the Pyr− cells may have been due to the accumulation of abnormal mitochondria, which produced less ATP, and that substrate for tricarboxylic acid cycle may use other metabolites, such as cytosolic NADH, amino acids, and pyruvate converted from glucose for the energy source of tricarboxylic acid cycle in the mitochondria.

In addition to the increase in OCR, the mitochondrial membrane potential (MMP) and ROS production showed an approximately 20% and approximately 50% increase, respectively, under pyruvate deprivation (Figure 2b and c). Given that an important consequence of abnormal mitochondria is ROS production, which has been implicated in the acceleration of aging, these results indicate that pyruvate deprivation induces the accumulation of abnormal mitochondria, resulting in increased ROS production. To investigate the mechanism behind the increase in OCR and MMP by pyruvate deprivation, we analyzed the expression of oxidative phosphorylation (OXPHOS) complexes and other mitochondrial proteins. Immunoblot analysis revealed that some components of OXPHOS complex III (ubiquinol-cytochrome C reductase core protein II) and IV (mitochondrially encoded cytochrome C oxidase I) were mainly accumulated in the OXPHOS complexes, and that uncoupling protein 2 (UCP2) levels were reduced in Pyr− cells; however, other mitochondrial proteins, such as VDAC1 and TOM20, remained unchanged (Figure 2d). These results suggest that increases in OCR and MMP in Pyr− cells are caused by the accumulation of OXPHOS complexes and the downregulation of UCP2, respectively.

Given that the downregulation of UCP2 is caused by the dysregulation of the NAD^+-SIRT1-PGC-1α axis in xeroderma pigmentosum group A-deficient cells (Fang et al., 2014), we

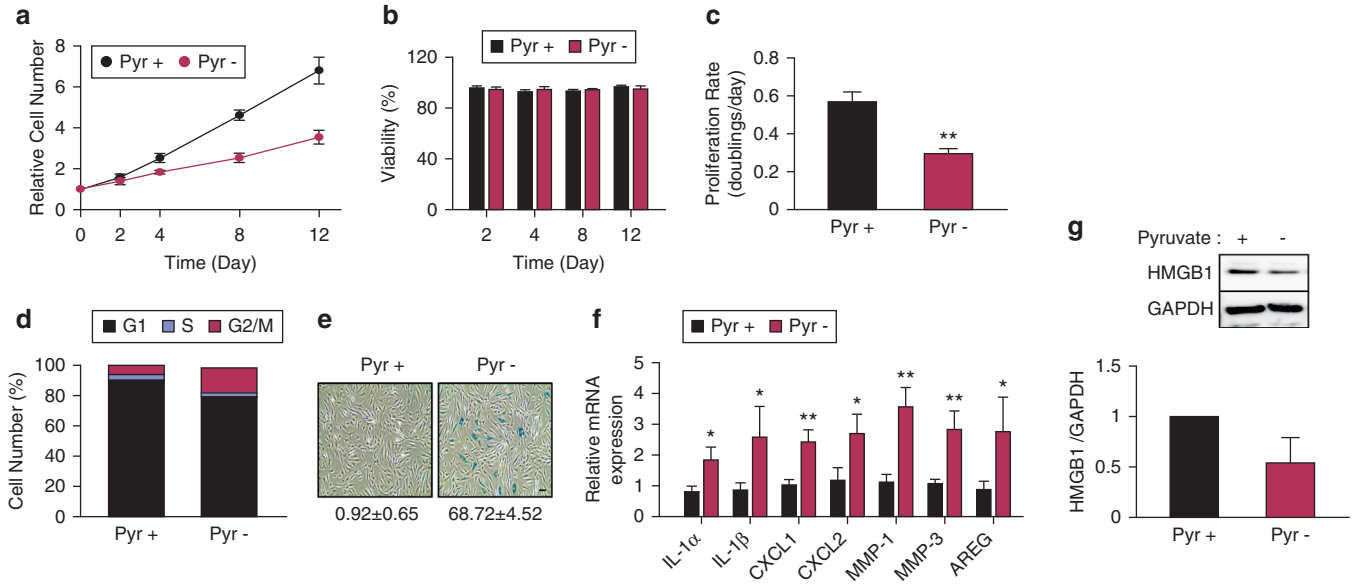

Figure 1. Pyruvate prevents cellular senescence in NHDFs. (**a**) NHDFs maintained in DMEM in the presence of 1 mM pyruvate to passage 3 were cultured in DMEM with (Pyr+) or without (Pyr−) 1 mM pyruvate at passage 4 and then counted at the indicated days. The relative cell number compared with day 0 was determined as the mean ± SD of one representative experiment (n = 3 wells), with three independent replicates. (**b**) The viability of the cells studied in (**a**) was assayed at the indicated days. Mean ± SD (n = 3). (**c**) The proliferation rate of the cells studied in (**a**) was assayed at 12 days. Mean ± SD (n = 3). $^{**}P < 0.01$ versus the corresponding value for Pyr+ cells. (**d**) NHDFs were cultured in DMEM with (Pyr+) or without (Pyr−) 1 mM pyruvate for 12 days, and the percentage of cells in each phase of the cell cycle was estimated by flow cytometric analysis. Data are representative of three experiments with similar results. (**e**) Pyr+ and Pyr− cells were subjected to SA-βgal staining. The percentages of SA-βgal-positive cells were quantified using Metamorph image-analysis software. Mean ± SD (n = 4). Scale bars = 50 μm. (**f**) Total RNA of Pyr+ and Pyr− cells were subjected to quantitative real-time reverse transcriptase PCR analysis of SASP genes. Mean ± SD (n = 3). $^{*}P < 0.05$, $^{**}P < 0.01$ versus the corresponding value for Pyr+ cells. (**g**) Immunoblot analysis of Pyr+ and Pyr− cells with antibodies to the HMGB1 and to GAPDH (loading control) (upper panel). The blot intensities of HMGB1 relative to GAPDH were determined as the mean ± SD from three independent experiments (lower panel). GAPDH, glyceraldehyde-3-phosphate dehydrogenase; HMGB1, high mobility group protein 1; MMP-1, matrix metalloproteinase-1; NHDF, normal human dermal fibroblast; SA-βgal, senescence-associated β-galactosidase; SASP, senescence-associated secretory phenotype; SD, standard deviation.

compared the amount of acetylated PGC-1α and other SIRT1 targets, RelA and p53. Immunoprecipitation analysis with anti-acetyl-lysine antibodies revealed that the amount of acetylated PGC-1α and RelA was considerably higher in Pyr− cells than in Pyr+ cells, whereas acetylated p53 remained unaffected (Figure 2e). UCP2 expression in Pyr+ cells transfected with PGC-1α small-interfering RNA (siRNA) was considerably lower than that in cells transfected with control siRNA, whereas the accumulation of OXPHOS complexes (ubiquinol-cytochrome C reductase core protein II and mitochondrially encoded cytochrome C oxidase I) in Pyr− cells was unaffected by PGC-1α knockdown (Figure 2f). These data indicate that the downregulation of UCP2 in Pyr− cells, which resulted in increased MMP, was caused by the acetylation of PGC-1α.

Mitochondrial activity, OCR is tightly connected with epigenetic profiles through the regulation of histone H3 lysine acetylation (Martinez-Reyes et al., 2016). In particular, acetylated histone H3 lysine 9 (H3K9ac), which is deacetylated by SIRT6 using NAD^+ as a cofactor, induces the expression of NF-κB target genes including inflammatory and SASP-related genes through NF-κB recruitment (Kawahara et al., 2009). The amount of H3K9ac was increased, and the interaction of SIRT6 with RelA, a subunit of NF-κB, was reduced by pyruvate deprivation (Supplementary Figure S5a and b online), resulting in an increase in NF-κB activity and the upregulation of NF-κB target genes including SOD2, IAP2, and ICAM (Supplementary Figure S5c and d) as well as SASP (Figure 1f). Given that acetylated RelA induces the transcriptional activity of NF-κB (Chen and Greene, 2004), these data suggest that pyruvate deprivation triggers NF-κB activation by increasing the acetylation of both H3K9 and RelA, and consequently upregulates SASP genes in NHDFs.

Pyruvate deprivation impairs cellular mitophagy

It has been reported that pyruvate is required for mitophagy via PINK1 stabilization, the initial step of mitophagy (Park et al., 2015). Therefore, we analyzed the mitochondrial contents in Pyr+ and Pyr− cells using Mitotracker green. Mitochondrial contents were increased approximately fourfold by pyruvate deprivation without affecting mitochondrial gene expression encoded from both the nucleus and the mitochondria (Figure 3a and Supplementary Figure S6a online), suggesting that the increase in mitochondrial contents in Pyr− cells may have been caused by defects in the mitochondrial clearance process, mitophagy. Immunoblot analysis showed that conversion of the LC3-I isoform to the more electrophoretically mobile LC3-II isoform during the formation of the autophagosome, as well as the accumulation of mitophagy-associated proteins including p62, PINK1, and Parkin, was increased by pyruvate deprivation; however, the levels of fusion and fission-related proteins such as Drp1, and Mitofusin-1 and -2, were unaffected (Figure 3b). In addition, pyruvate deprivation attenuated bafilomycin-induced autophagy flux arrest (Figure 3c and d) and TOM20 degradation after treatment with the uncouplers, FCCP and CCCP (Figure 3e). These data show that pyruvate

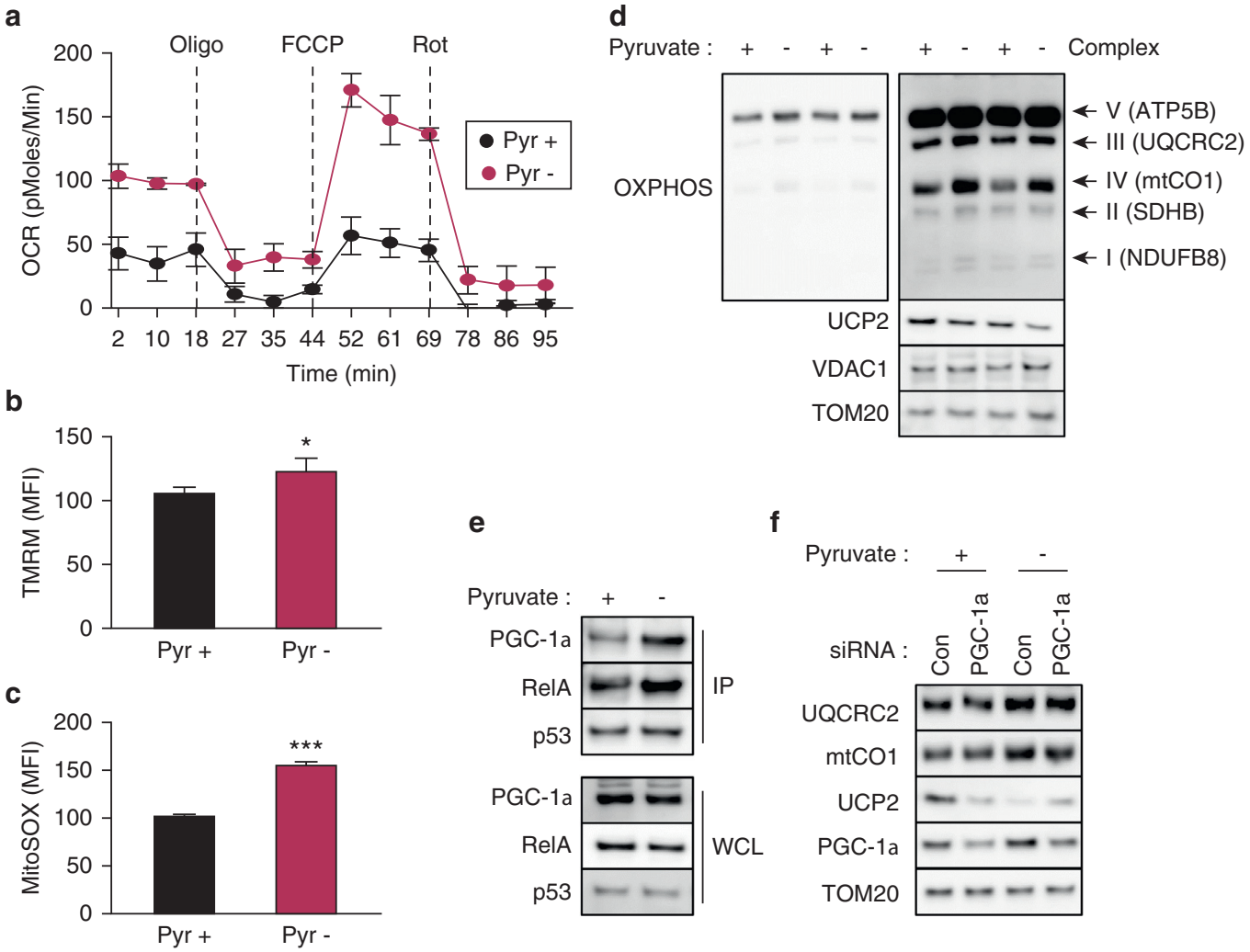

Figure 2. Pyruvate deprivation induces an accumulation of abnormal mitochondria. (**a**) Pyr+ and Pyr− cells were analyzed to determine the oxygen consumption rate (OCR). Mean ± SD (n = 3). (**b, c**) Pyr+ and Pyr− cells were stained with TMRM or MitoSOX for the detection of mitochondrial membrane potential (MMP) (**b**) or mitochondrial ROS (**c**), respectively, and analyzed using flow cytometry. Mean ± SD (n = 3). $*P < 0.05$, $***P < 0.001$ versus the corresponding value for Pyr+ cells. (**d**) Immunoblot analysis of Pyr+ and Pyr− cells with antibodies to anti-OXPHOS (complex I–V) and to the indicated mitochondrial proteins. Two different blot exposures are shown for OXPHOS. The images represent two samples from each group and are representative of three independent experiments. (**e**) Lysates of Pyr+ and Pyr− cells were subjected to immunoprecipitation with antibodies to acetyl-lysine, and the resulting precipitates (IP) as well as the whole-cell lysates (WCL) were subjected to immunoblot analysis with antibodies to PGC-1α, RelA, and p53. (**f**) Pyr+ and Pyr− cells were transfected with control (Con) or PGC-1α siRNA, and further incubated with each culture media for 2 days. The lysates of the NHDFs were subjected to immunoblot analysis with antibodies to the indicated proteins. mtCO1, mitochondrially encoded cytochrome C oxidase I, NHDF, normal human dermal fibroblast; OXPHOS, oxidative phosphorylation; PGC-1α, peroxisome proliferator-activated receptor gamma coactivator 1-α; RelA, NF-κB p65 subunit; ROS, reactive oxygen species; siRNA, small-interfering RNA; SD, standard deviation; UCP2, uncoupling protein 2; UQCRC2, ubiquinol-cytochrome C reductase core protein II.

controls the basal autophagic, specifically mitophagic, flux of NHDFs. To confirm the effect of pyruvate on mitophagy, we analyzed the change in fluorescence in mitochondria-targeted mKeima, which has an excitation spectrum that changes from mitochondria in the cytoplasm (neutral pH, ex 440 nm) to mitochondria in acidic lysosomes (acidic pH, ex 550 nm) (Kogure et al., 2006). The basal mitochondria-targeted mKeima signal (550ex:440ex) was elevated approximately threefold in Pyr− cells compared with that in Pyr+ cells treated with CCCP; the mitochondria-targeted mKeima signal in Pyr− cells was not changed by treatment with CCCP (Figure 3f and Supplementary Figure S6b). Taken together, these findings suggest that pyruvate is required for mitophagy in the process of degradation of abnormal mitochondria after autolysosome formation. Therefore, we speculated that the increase in OCR and OXPHOS complexes due to pyruvate deprivation was caused by mitophagic defects in the step following autolysosome formation.

Pyruvate deprivation promotes lysosomal inactivation via an increase in acetylated v-ATPaseV0A1

In addition to the accumulation of abnormal mitochondria and the dysregulation of mitophagy in Pyr− cells, electron microscopy studies revealed striking levels of intracellular vesiculation relative to those in Pyr+ cells (Figure 4a). Using lysotracker red (Figure 4b) and by measuring lysosomal-associated membrane protein 1 (LAMP1) levels, it was confirmed that lysosome formation was induced in Pyr− cells (Supplementary Figure S7a and b online). Lysosomal biogenesis is mainly regulated by transcription factor EB (TFEB), which is translocated from the cytosol to the nucleus under

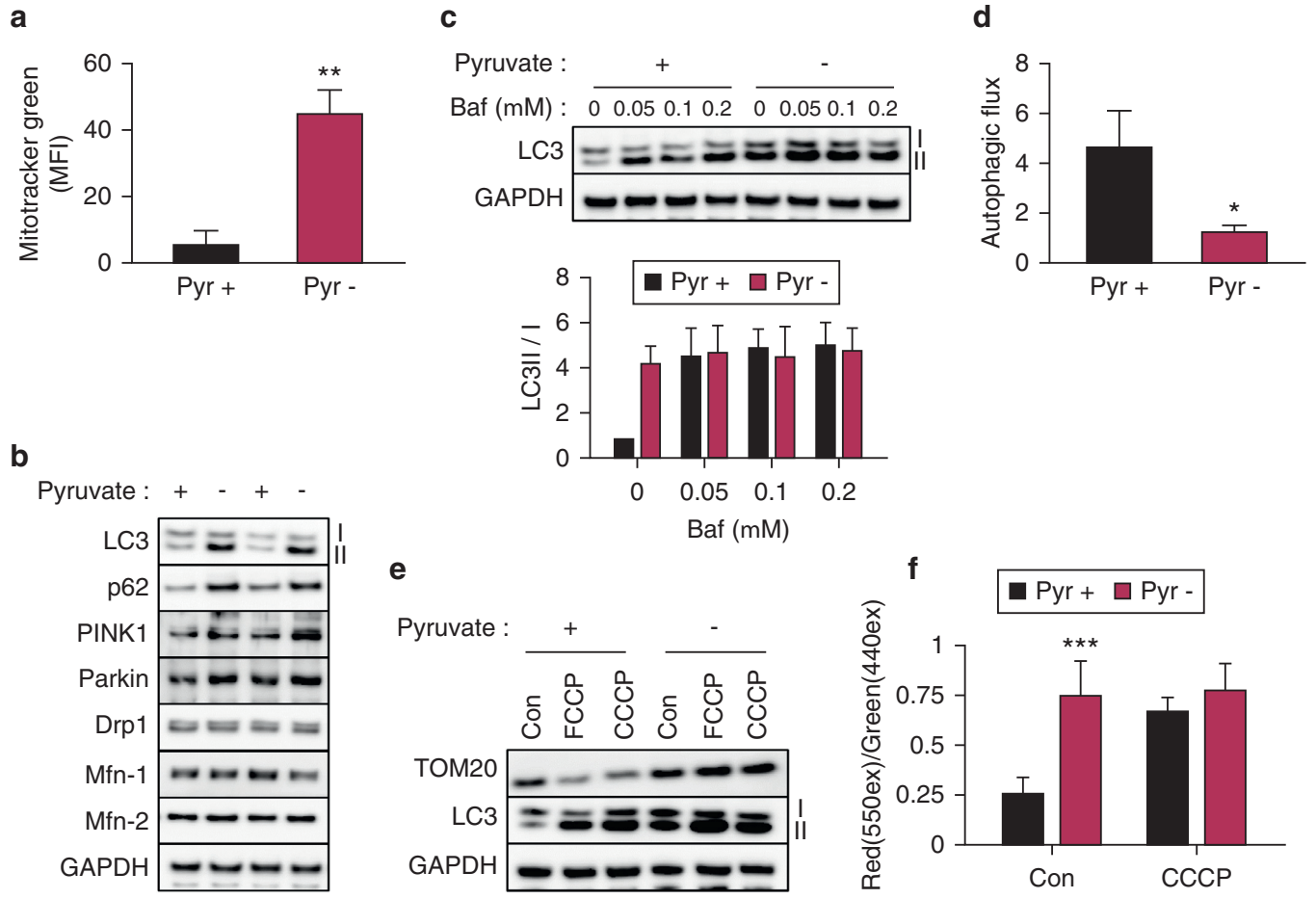

Figure 3. Pyruvate deprivation impairs cellular mitophagy. (**a**) The mitochondrial contents of Pyr+ and Pyr− cells were analyzed using Mitotracker green. Mean ± SD (n = 3). $^{**}P < 0.01$ versus the corresponding value for Pyr+ cells. (**b**) Immunoblot analysis of Pyr+ and Pyr− cells with the indicated antibodies. (**c**) Pyr+ and Pyr− cells were treated with DMSO (0) or the indicated dose of bafilomycin (Baf) for 24 hours, after which the lysates were subjected to immunoblot analysis with antibodies to LC3 and to GAPDH (upper panel). The blot intensities of LC3-II relative to those of LC3-I were determined as the mean ± SD from three independent experiments (lower panel). (**d**) Autophagy flux was calculated as the difference in LC3-II/I expression between cells cultured with DMSO and 0.1 μM bafilomycin in (**c**). Mean ± SD (n = 3). $^{*}P < 0.05$ versus the corresponding value for Pyr+ cells. (**e**) Pyr+ and Pyr− cells were treated with DMSO (Con), 10 μM FCCP, or 10 μM CCCP for 24 hours, after which the lysates were subjected to immunoblot analysis with antibodies to TOM20, LC3, and GAPDH. (**f**) Quantification of the ratio (550ex:440ex) of high signal area (red) to total mitochondrial area (green) in Pyr+ and Pyr− cells treated with DMSO (Con) or 10 μM CCCP (>30 cells per group in two independent experiments) was estimated from Supplementary Figure S6b. $^{***}P < 0.001$ versus the corresponding value for Pyr+ cells. GAPDH, glyceraldehyde-3-phosphate dehydrogenase; SD, standard deviation.

conditions of starvation, as well as lysosomal or mitochondrial stress (Baixauli et al., 2015; Brisson et al., 2016). Therefore, we analyzed the localization and activation of TFEB. The activation of TFEB was accompanied by an increase in the amount of TFEB in the nucleus as detected by both subcellular fractionation (Supplementary Figure S7c) and immunofluorescence staining (Supplementary Figure S7d), and by the upregulation of its target genes in Pyr− cells (Supplementary Figure S7e), suggesting that pyruvate deprivation induces lysosomal biogenesis via the activation of TFEB.

During mitophagy, the autophagosome fuses with the lysosome for the clearance of abnormal mitochondria; impairment of autophagy caused by lysosomal inactivation induces premature senescence (Carmona-Gutierrez et al., 2016). Given that the amount of mitochondria-containing autolysosomes is elevated in Pyr− cells, we speculated that the accumulation of the autolysosome may be caused by the inactivation of lysosome. Therefore, we measured the lysosomal pH, which is maintained at approximately pH 4–5 for the activation of various hydrolases. Measurement with DND-160, a specific lysosomal pH-sensitive probe, revealed that lysosomal pH was substantially increased in Pyr− cells (Figure 4c). Accompanying the increase of lysosomal pH, degradation of the lysosomal substrate DQ-BSA was decreased by approximately 40% in Pyr− cells (Figure 4d). In addition, the levels of OXPHOS complexes (ubiquinol-cytochrome C reductase core protein II and mitochondrially encoded cytochrome C oxidase I), LAMP1, and LC3-II in Pyr+ cells were increased by treatment with bafilomycin to levels equivalent to those in untreated Pyr− cells, whereas the level of UCP2 was unaffected (Supplementary Figure S7f). These data suggest that the increase in lysosomal biogenesis is caused by a compensatory mechanism to improve lysosomal inactivation due to pyruvate deprivation.

Next, we wondered how the lysosome is inactivated in Pyr− cells. LDH has bidirectional activity for the conversion of pyruvate and lactate through tetrameric composition of two different subunits, LDH-A and LDH-B, which have

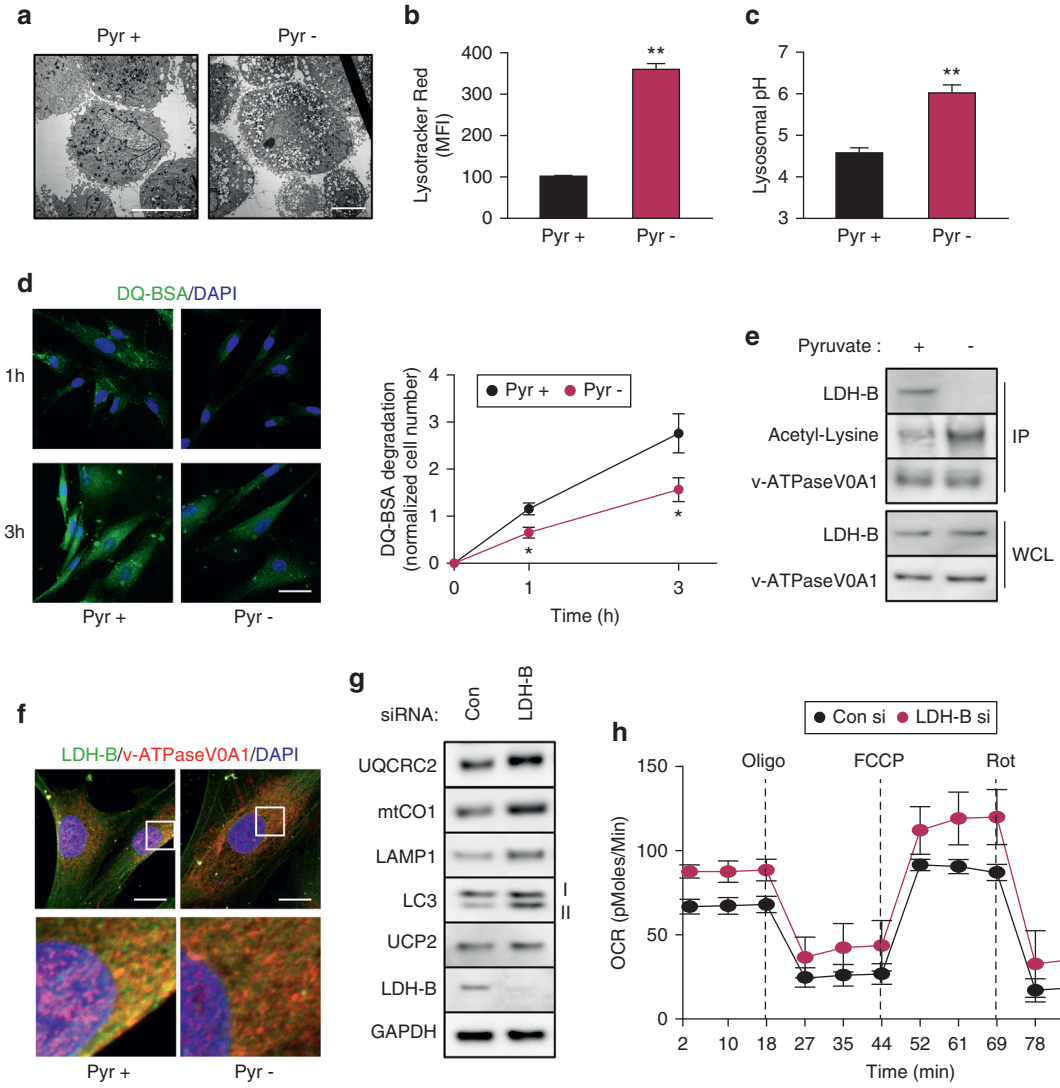

Figure 4. Pyruvate deprivation promotes lysosomal inactivation by increasing acetylated v-ATPaseV0A1. (**a**) Pyr+ and Pyr− cells were subjected to electron microscopy. Scale bar = 10 μm. (**b**) Pyr+ and Pyr− cells were stained with lysotracker red and then analyzed using flow cytometry. Mean ± SD (n = 3). $^{**}P < 0.01$ versus the corresponding value for Pyr+ cells. (**c**) The lysosomal pH of Pyr+ and Pyr− cells was analyzed using DND-160. Mean ± SD (n = 3). $^{**}P < 0.01$ versus the corresponding value for Pyr+ cells. (**d**) The lysosomal activity of Pyr+ and Pyr− cells was analyzed using DQ-BSA dequenching after incubation for 1 or 3 hours (left panel). The relative fluorescence level was analyzed by quantification using Imaris (right panel). Scale bars = 20 μm. Mean ± SD (n = 3). $^{*}P < 0.05$ versus the corresponding value for Pyr+ cells. (**e**) Lysates of Pyr+ and Pyr− cells were subjected to immunoprecipitation with antibodies to v-ATPaseV0A1, and the resulting precipitates (IP) as well as the whole-cell lysates (WCL) were subjected to immunoblot analysis with the indicated antibodies. (**f**) Pyr+ and Pyr− cells were subjected to immunofluorescence analysis with antibodies to LDH-B and v-ATPaseV0A1. The areas indicated by the box are shown at a higher magnification below. Scale bar = 10 μm. (**g, h**) NHDFs cultured in DMEM with 1 mM pyruvate were transfected with control (Con) or LDH-B siRNA and further incubated in culture media for 2 days. Lysates of the NHDFs were subjected to immunoblot analysis with antibodies to the indicated proteins (**g**), and NHDFs were analyzed to determine the OCR (**h**). Mean ± SD (n = 3). GAPDH, glyceraldehyde-3-phosphate dehydrogenase; LDH, lactate dehydrogenase; NHDF, normal human dermal fibroblast; OCR, oxygen consumption rate; SA-βgal, senescence-associated β-galactosidase; SD, standard deviation; siRNA, small-interfering RNA; UCP2, uncoupling protein 2; v-ATPase, vacuolar-type H^+-ATPase.

a higher affinity for pyruvate and lactate, respectively (Doherty and Cleveland, 2013). Pyruvate is converted to lactate by LDH-A, and LDH-B converts lactate back to pyruvate while interacting with v-ATPase, especially v-ATPaseV0A1, to yield H^+, which is used for the acidification of lysosomes (Brisson et al., 2016). Interestingly, the interaction of LDH-B with v-ATPaseV0A1 was disrupted (Figure 4e) and colocalization was also reduced in the Pyr− cells (Figure 4f). In addition, the amount of acetylated v-ATPaseV0A1 was increased in Pyr− cells compared with that in Pyr+ cells (Figure 4e). Immunoprecipitation with anti-acetyl-lysine antibodies confirmed that v-ATPaseV0A1 was acetylated (Supplementary Figure S7g) and that this acetylation was accumulated by SIRT1 knockdown or by treatment with the deacetylase inhibitors, trichostatin A and nicotinamide (Supplementary Figure S7h). These data suggest that the interaction between LDH-B and v-ATPaseV0A1 is sensitive to the decrease in NAD^+ and may be caused by the acetylation of v-ATPaseV0A1, which is deacetylated by SIRT1. Moreover, the amounts of OXPHOS complexes (ubiquinol-cytochrome C reductase core protein II and mitochondrially encoded cytochrome C oxidase I), LAMP1,

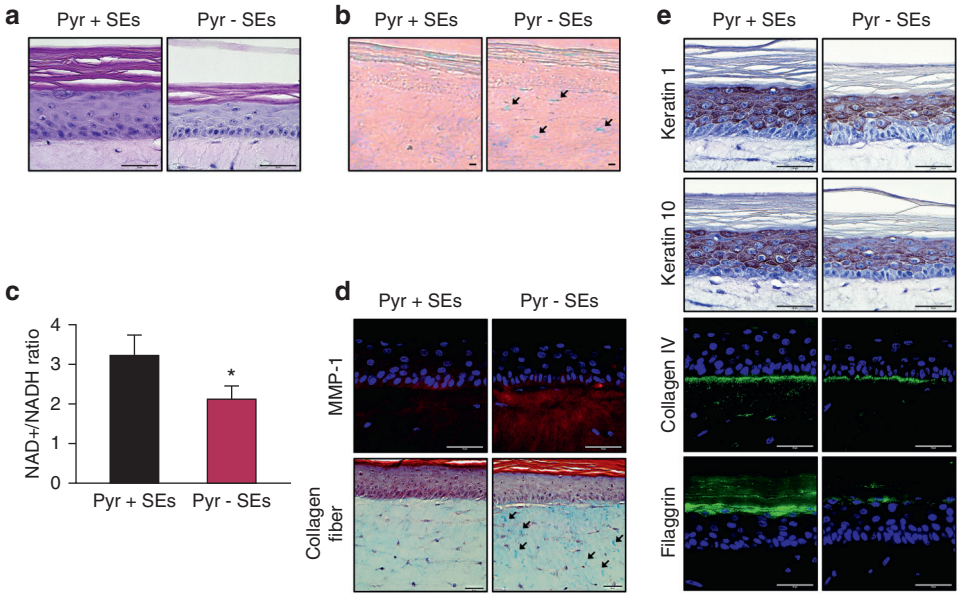

Figure 5. Pyruvate enhances the differentiation of skin epidermis by preventing aging phenotypes of skin dermis. (**a**–**e**) Skin equivalents (SEs) were subjected to hematoxylin and eosin staining (**a**), to SA-βgal staining—arrows indicate SA-βgal-positive cells (**b**), to analysis of the NAD^+/NADH ratio in dermal fibroblasts (**c**), to immunohistochemistry with antibodies to MMP-1 and Masson's trichrome staining for detection of pan-collagen fiber—arrows indicate aggregated and abnormal collagen fiber (**d**), and to immunohistochemistry with antibodies to epidermal differentiation markers (**e**). Scale bars = 50 μm. MMP-1, matrix metalloproteinase-1; NAD^+, oxidized nicotinamide adenine dinucleotide; NADH, reduced nicotinamide adenine dinucleotide; SA-βgal, senescence-associated β-galactosidase.

and LC3-II in Pyr+ cells transfected with LDH-B siRNA were higher than those in Pyr+ cells transfected with control siRNA, at levels similar to those observed in untreated Pyr− cells or Pyr+ cells treated with bafilomycin; however, UCP2 levels were unaffected (Figure 4g and Supplementary Figure S7f). Consistent with the accumulation of OXPHOS complexes, the basal and maximum OCR were increased by the knockdown of LDH-B (Figure 4h and Supplementary Figure S7i). These data suggest that the interaction of LDH-B with v-ATPV0A1 to supply protons for maintaining lysosomal activity is disrupted under pyruvate deprivation conditions, resulting in the promotion of the accumulation of abnormal mitochondria by mitophagy defect and consequent cellular senescence.

Pyruvate promotes antiaging phenotypes in skin equivalents

Skin aging is a complex phenomenon induced by extrinsic or intrinsic factors, and is characterized by flattening of the epidermal-dermal interface and breakdown of the dermal tissue, resulting in the problems in development of the epidermis (Farage et al., 2008). To identify the effect of pyruvate on human skin aging, we used the skin equivalent (SE) model, which closely mimics in vivo human skin, cultured in the presence (Pyr+ SEs) or absence (Pyr− SEs) of pyruvate for 7 days after exposure to air. Histological analysis of the SEs revealed that the epidermis, including the stratum corneum, of Pyr− SEs was thinner than that of Pyr+ SEs (Figure 5a). Although the morphology and number of dermal cells were not substantially changed, the number of senescence-associated β-galactosidase-positive cells was increased and the NAD^+/NADH ratio was decreased in the dermis of Pyr− SEs compared with those in the dermis of Pyr+ SEs (Figure 5b and c). Moreover, the levels of matrix metalloproteinase-1, also known as fibroblast collagenase, and SASP were markedly elevated and aggregated, and abnormal collagen fiber were increased in the dermis of Pyr− SEs, as previously described in aged skin (Fligiel et al., 2003) (Figure 5d), suggesting that pyruvate also protects against senescence in dermal fibroblasts in SEs.

In addition, we compared the levels of markers of keratinocyte differentiation such as keratin 1, keratin 10, and

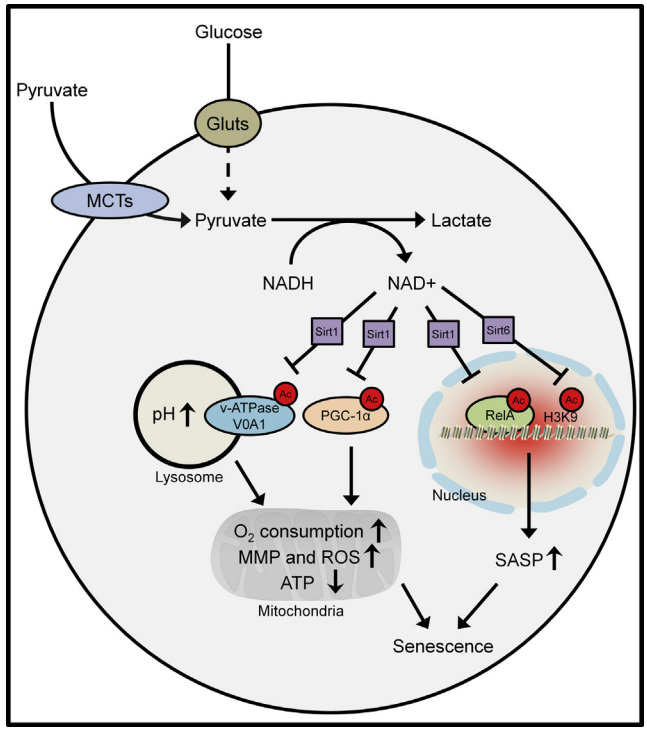

Figure 6. A model illustrating the physiological function of pyruvate underlying its protective role against cellular senescence. See the Discussion section for details. H3K9, histone H3 lysine 9; MCT, monocarboxylate transporter; MMP, mitochondrial membrane potential; NAD^+, oxidized nicotinamide adenine dinucleotide; NADH, reduced nicotinamide adenine dinucleotide; PGC-1α, peroxisome proliferator-activated receptor gamma coactivator 1-α; RelA, NF-κB p65 subunit; ROS, reactive oxygen species; SASP, senescence-associated secretory phenotype; v-ATPase, vacuolar-type H^+-ATPase.

filaggrin, and a marker of the basement membrane, collagen IV, in the dermoepidermal junction. These markers are known to be upregulated according to the stage of keratinocyte differentiation. Immunohistochemical analysis revealed that all of these markers were markedly reduced in Pyr− SEs compared with those in Pyr+ SEs (Figure 5e); however, the differentiation of HaCat cells—immortalized human keratinocytes—was unchanged in the presence or absence of pyruvate (Supplementary Figure S8 online). Because the epidermis is regulated by dermal fibroblasts (Maas-Szabowski et al., 1999), these data suggest that senescence in dermal fibroblasts due to pyruvate deprivation triggers the deregulation of development in epidermal keratinocytes; this is similar to the mechanism of skin aging.

DISCUSSION

Despite its low concentration (approximately 30 μM) in human blood plasma, pyruvate is often used as a supplement at supraphysiological concentrations of 1 mM in traditional synthetic cell culture media, which were not developed with the primary goal of mimicking human blood plasma, but rather to supply large amounts of media (Cantor et al., 2017). Many groups have used pyruvate in synthetic cell culture media as an efficient energy source that directly enters the mitochondria without glycolysis. However, pyruvate has a protective role against mitochondrial dysfunction by inducing aspartate synthesis through NAD^+ generation during the conversion of pyruvate to lactate by LDH-A (Birsoy et al., 2015; Cardaci et al., 2015; Sullivan et al., 2015). Therefore, we propose that in vitro cultured cells with higher concentrations of pyruvate may show different metabolic rates and processes than cells under in vivo conditions with lower concentrations of pyruvate.

On the basis of our findings, we propose a model for the mechanism underlying the connection between pyruvate metabolism and senescence (Figure 6). Pyruvate, which is imported through monocarboxylate transporters into the cells, inhibits senescence in dermal fibroblasts in both primary cell culture and 3D SE model systems. NAD^+, which is generated during the conversion of pyruvate to lactate by LDH-A, induces the deacetylation of SIRT1 targets such as PGC-1α, RelA, and v-ATPaseV0A1, and the deacetylation of an SIRT6 target, H3K9ac. Under pyruvate deprivation conditions, the accumulation of acetylated PGC-1α induces the downregulation of UCP2, resulting in the elevation of the MMP, as well as the accumulation of acetylated v-ATPaseV0A1, and disruption of its interaction with LDH-B; this induces the dysregulation of lysosomal acidification, resulting in a series of events including mitophagy defects, the accumulation of abnormal mitochondria, an increase in mitochondrial ROS production, and the upregulation of SASP, which is induced by a combination of acetylated RelA and H3K9.

Recently, the control of aging or aging-related diseases to improve overall health or lifespan has been attempted using NAD^+ precursor supplements (Fang et al., 2014; Imai and Guarente, 2014; Mills et al., 2016). The accumulation of senescent dermal fibroblasts in the skin induces dysregulated keratinocyte differentiation, resulting in increased inflammation and a decrease in the thickness of the skin, in particular dermal layer. Here, we propose that pyruvate can be used as an antisenescence metabolite that may improve skin aging through the control of mitochondrial and lysosomal function via NAD^+ generation in dermal fibroblasts, without side effects. In addition to the senescence-induced problems of skin tissues, because pyruvate concentrations are much lower in human blood plasma than in in vitro cell culture systems, it may be interesting to determine in a future study whether in vivo cells can obtain pyruvate by direct consumption to prevent aging or aging-related diseases, and whether natural aging is induced by pyruvate deprivation in vivo. Consequently, it may be necessary to consider therapies that increase cellular pyruvate levels in vivo.

MATERIALS AND METHODS

Reagents

Antibodies to high mobility group protein 1, OXPHOS, RelA, SIRT6, H3K9ac, H3, Mfn-1, LDH-B, LAMP1, and matrix metalloproteinase-1 were purchased from Abcam (Cambridge, UK); those to UCP2, AMPK phosphorylated on Thr^{172}, total AMPK, SIRT6, p62, PINK1, Parkin, Mfn-2, TFEB, acetyl-lysine, and PARP-1 were purchased from Cell Signaling Technology (Danvers, MA); those to GAPDH, VDAC1, TOM20, PGC-1α, v-ATPaseV0A1, α-tubulin, and collagen IV were purchased from Santa Cruz Biotechnology (Dallas, TX); those to LC3 were purchased from Novus Biologicals (Littleton, CO); those to p53 were purchased from Agilent Technologies (Santa Clara, CA); those to filaggrin were purchased from Leica Biosystems (Newcastle, UK); and those to keratin 1 and keratin 10 were purchased from Covance (Princeton, NJ). Sodium pyruvate, aspartic acid, α-ketobutyric acid, nicotinamide mononucleotide, bafilomycin, DMSO, CCCP, FCCP, rotenone, UK5099, trichostatin A, and nicotinamide were obtained from Sigma Aldrich (St. Louis, MO). TMRM, mitoSOX, Mitotracker green FM, Mitotracker red CMXRos, Lysotracker red DND-99, LysoSensor yellow/blue DND-160, and DQ-green BSA were purchased from Invitrogen (Carlsbad, CA).

Cell culture

NHDFs were purchased from Lonza (Basel, Switzerland) and maintained in DMEM supplemented with 10% fetal bovine serum, 1% penicillin/streptomycin mixture, and 4 mM L-glutamine in the absence or presence of 1 mM pyruvate. The NHDFs were transfected with siRNA for green fluorescent protein (control) or target genes using the Neon Transfection System (Invitrogen) after detaching the cells from the culture plate. At 1 or 2 days after transfection, cells were used for further experiments. The control siRNA for green fluorescent protein was obtained from Samchully Pharm (Seoul, Korea). PGC-1α siRNA was purchased from Santa Cruz Biotechnology. SIRT1 siRNA was purchased from Cell Signaling Technology. SLC16A6 and LDH-B siRNA were purchased from Bioneer (Seoul, Korea). HaCat, a spontaneously immortalized keratinocyte cell line, was obtained from Cell Lines Service (Eppelheim, Germany) and maintained in DMEM supplemented with 10% fetal bovine serum, 1% penicillin/streptomycin mixture, and 4 mM L-glutamine in the presence of 1 mM pyruvate. For the analysis of differentiation, HaCat cells were incubated in DMEM in the absence or presence of 1 mM pyruvate for the indicated time periods.

CONFLICT OF INTEREST

The authors state no conflict of interest.

ACKNOWLEDGMENTS

This study was supported by the Basic Science Research Program through the National Research Foundation of Korea funded by the Ministry of Education (NRF-2013R1A6A3A04057678 to ISK) and by a grant of the Korea Healthcare

technology R&D Project, Ministry of Health & Welfare, Republic of Korea (HN15C0102 to A-YL).

SUPPLEMENTARY MATERIAL

Supplementary material is linked to the online version of the paper at www.jidonline.org, and at https://doi.org/10.1016/j.jid.2018.05.033.

REFERENCES

Baixauli F, Acin-Perez R, Villarroya-Beltri C, Mazzeo C, Nunez-Andrade N, Gabande-Rodriguez E, et al. Mitochondrial respiration controls lysosomal function during inflammatory T cell responses. Cell Metab 2015;22:485–98.

Birsoy K, Wang T, Chen WW, Freinkman E, Abu-Remaileh M, Sabatini DM. An essential role of the mitochondrial electron transport chain in cell proliferation is to enable aspartate synthesis. Cell 2015;162:540–51.

Brisson L, Banski P, Sboarina M, Dethier C, Danhier P, Fontenille MJ, et al. Lactate dehydrogenase B controls lysosome activity and autophagy in cancer. Cancer Cell 2016;30:418–31.

Camacho-Pereira J, Tarrago MG, Chini CC, Nin V, Escande C, Warner GM, et al. CD38 dictates age-related NAD decline and mitochondrial dysfunction through an SIRT3-dependent mechanism. Cell Metab 2016;23:1127–39.

Cantor JR, Abu-Remaileh M, Kanarek N, Freinkman E, Gao X, Louissaint A Jr, et al. Physiologic medium rewires cellular metabolism and reveals uric acid as an endogenous inhibitor of UMP synthase. Cell 2017;169:258–272.e17.

Cardaci S, Zheng L, MacKay G, van den Broek NJ, MacKenzie ED, Nixon C, et al. Pyruvate carboxylation enables growth of SDH-deficient cells by supporting aspartate biosynthesis. Nat Cell Biol 2015;17:1317–26.

Carmona-Gutierrez D, Hughes AL, Madeo F, Ruckenstuhl C. The crucial impact of lysosomes in aging and longevity. Ageing Res Rev 2016;32:2–12.

Chen LF, Greene WC. Shaping the nuclear action of NF-kappaB. Nat Rev Mol Cell Biol 2004;5:392–401.

Doherty JR, Cleveland JL. Targeting lactate metabolism for cancer therapeutics. J Clin Invest 2013;123:3685–92.

Fang EF, Scheibye-Knudsen M, Brace LE, Kassahun H, SenGupta T, Nilsen H, et al. Defective mitophagy in XPA via PARP-1 hyperactivation and NAD(+)/SIRT1 reduction. Cell 2014;157:882–96.

Farage MA, Miller KW, Elsner P, Maibach HI. Intrinsic and extrinsic factors in skin ageing: a review. Int J Cosmet Sci 2008;30:87–95.

Fligiel SE, Varani J, Datta SC, Kang S, Fisher GJ, Voorhees JJ. Collagen degradation in aged/photodamaged skin in vivo and after exposure to matrix metalloproteinase-1 in vitro. J Invest Dermatol 2003;120:842–8.

Harris M. Pyruvate blocks expression of sensitivity to antimycin A and chloramphenicol. Somatic Cell Genet 1980;6:699–708.

Horan MP, Pichaud N, Ballard JW. Review: quantifying mitochondrial dysfunction in complex diseases of aging. J Gerontol A Biol Sci Med Sci 2012;67:1022–35.

Imai S, Guarente L. NAD+ and sirtuins in aging and disease. Trends Cell Biol 2014;24:464–71.

Kawahara TL, Michishita E, Adler AS, Damian M, Berber E, Lin M, et al. SIRT6 links histone H3 lysine 9 deacetylation to NF-kappaB-dependent gene expression and organismal life span. Cell 2009;136:62–74.

King MP, Attardi G. Human cells lacking mtDNA: repopulation with exogenous mitochondria by complementation. Science 1989;246:500–3.

Kogure T, Karasawa S, Araki T, Saito K, Kinjo M, Miyawaki A. A fluorescent variant of a protein from the stony coral Montipora facilitates dual-color single-laser fluorescence cross-correlation spectroscopy. Nat Biotechnol 2006;24:577–81.

Kuilman T, Michaloglou C, Mooi WJ, Peeper DS. The essence of senescence. Genes Dev 2010;24:2463–79.

Lopez-Otin C, Blasco MA, Partridge L, Serrano M, Kroemer G. The hallmarks of aging. Cell 2013;153:1194–217.

Maas-Szabowski N, Shimotoyodome A, Fusenig NE. Keratinocyte growth regulation in fibroblast cocultures via a double paracrine mechanism. J Cell Sci 1999;112(Pt 12):1843–53.

Martinez-Reyes I, Diebold LP, Kong H, Schieber M, Huang H, Hensley CT, et al. TCA cycle and mitochondrial membrane potential are necessary for diverse biological functions. Mol Cell 2016;61:199–209.

Mills KF, Yoshida S, Stein LR, Grozio A, Kubota S, Sasaki Y, et al. Long-term administration of nicotinamide mononucleotide mitigates age-associated physiological decline in mice. Cell Metab 2016;24:795–806.

Park S, Choi SG, Yoo SM, Nah J, Jeong E, Kim H, et al. Pyruvate stimulates mitophagy via PINK1 stabilization. Cell Signal 2015;27:1824–30.

Park S, Kim K, Bae IH, Lee SH, Jung J, Lee TR, et al. TIMP3 is a CLOCK-dependent diurnal gene that inhibits the expression of UVB-induced inflammatory cytokines in human keratinocytes. FASEB J 2018;32:1510–23.

Sullivan LB, Gui DY, Hosios AM, Bush LN, Freinkman E, Vander Heiden MG. Supporting aspartate biosynthesis is an essential function of respiration in proliferating cells. Cell 2015;162:552–63.

Wiley CD, Velarde MC, Lecot P, Liu S, Sarnoski EA, Freund A, et al. Mitochondrial dysfunction induces senescence with a distinct secretory phenotype. Cell Metab 2016;23:303–14.

Yun J, Finkel T. Mitohormesis. Cell Metab 2014;19:757–66.

Zhang H, Ryu D, Wu Y, Gariani K, Wang X, Luan P, et al. NAD(+) repletion improves mitochondrial and stem cell function and enhances life span in mice. Science 2016;352:1436–43.